Context-dependent and dynamic functional influence of corticothalamic pathways to first- and higher-order visual thalamus

Megan A. Kirchgessner[a,b], Alexis D. Franklin[a], and Edward M. Callaway[a,b,1]

[a]Systems Neurobiology Laboratories, Salk Institute for Biological Studies, La Jolla, CA 92037; and [b]Neurosciences Graduate Program, University of California San Diego, La Jolla, CA 92093

Contributed by Edward M. Callaway, April 3, 2020 (sent for review February 4, 2020; reviewed by Martha E. Bickford and S. Murray Sherman)

Layer 6 (L6) is the sole purveyor of corticothalamic (CT) feedback to first-order thalamus and also sends projections to higher-order thalamus, yet how it engages the full corticothalamic circuit to contribute to sensory processing in an awake animal remains unknown. We sought to elucidate the functional impact of L6CT projections from the primary visual cortex to the dorsolateral geniculate nucleus (first-order) and pulvinar (higher-order) using optogenetics and extracellular electrophysiology in awake mice. While sustained L6CT photostimulation suppresses activity in both visual thalamic nuclei in vivo, moderate-frequency (10 Hz) stimulation powerfully facilitates thalamic spiking. We show that each stimulation paradigm differentially influences the balance between monosynaptic excitatory and disynaptic inhibitory corticothalamic pathways to the dorsolateral geniculate nucleus and pulvinar, as well as the prevalence of burst versus tonic firing. Altogether, our results support a model in which L6CTs modulate first- and higher-order thalamus through parallel excitatory and inhibitory pathways that are highly dynamic and context-dependent.

corticothalamic | pulvinar | dLGN | TRN | optogenetics

While the flow of information from the thalamus to the cortex is widely appreciated as a critical step in sensory processing, the significance of a given cortical area's projection back to the thalamus is considerably less clear. In the case of first-order nuclei, like the dorsolateral geniculate nucleus (dLGN) in the visual system, this corticothalamic feedback originates from layer 6 (L6). L6 corticothalamic neurons (L6CTs) have been classically described as providing "modulatory" feedback to the dLGN (1, 2) that may influence response gain (3–8), temporal precision (9, 10), spatiotemporal filtering (6, 10, 11), sensory adaptation (12), and burst versus tonic firing modes (7, 8, 11, 12). Still, how these L6CTs might perform these various functions is not well understood. Moreover, many L6CTs also project to higher-order thalamus, such as the visual pulvinar (also known as the lateral-posterior nucleus, or LP, in rodents) (13). While anatomical and physiological similarities between L6CT projections to first- and higher-order thalamus (14–16) suggest they may play similar "modulatory" functions across thalamic nuclei classes, the pathway from cortex to higher-order thalamus has not been investigated in vivo. Thus, many questions remain with regard to the nature of corticothalamic feedback as a general feature of sensory circuits and whether these same principles hold across different classes of thalamic nuclei.

One such question is how L6CTs influence their thalamic targets during sensory processing in an awake animal. On one hand, previous observations of dramatically reduced visual responses recorded in the dLGN of anesthetized mice during V1 L6CT optogenetic activation (4, 5) suggest that L6CT feedback may be fundamentally inhibitory, likely through a disynaptic inhibitory pathway through the GABAergic thalamic reticular nucleus (TRN). However, other studies in the visual as well as other sensory systems disagree, finding no change or even increased activity in first-order thalamus with L6CT photoactivation (10, 17, 18). Moreover, optogenetically inactivating L6CTs has mixed effects in the dLGN (5), suggesting that their natural function is not to invariably suppress their thalamic targets.

An alternative explanation could be that the level and manner of L6CTs' activation may determine how they influence their thalamic targets. For example, the effects of L6CT optogenetic stimulation on the first-order ventral posterior medial nucleus (VPm) in the somatosensory in vitro slice preparation have been shown to "switch" from being net-suppressing to net-facilitating with higher-frequency (10 Hz) L6CT stimulation (19). This frequency-dependence has been explained by the different short-term plasticity characteristics at different synapses in the full corticothalamic circuit, since the competing monosynaptic excitatory and disynaptic inhibitory (via the TRN) routes to first-order thalamus are net-facilitating and net-depressing, respectively (19). Previous studies have not used temporally controlled L6CT optogenetic manipulations in awake animals or probed in vivo L6CT effects on a higher-order thalamic nucleus. Therefore, it remains to be seen whether L6CT projections can exert flexible, bidirectional influence on thalamic activity in the visual system, in different classes of thalamic nuclei, and in vivo.

To address these questions, we have recorded extracellular single-unit activity from the dLGN, pulvinar, and TRN in awake mice. We optogenetically manipulated L6CTs in the primary visual cortex with both controlled (photostimulation trains) and uncontrolled (continuous light) methods for photostimulation.

Significance

Layer 6 corticothalamic (L6CT) projections play important modulatory roles in thalamic processing, yet how this modulation is executed is unclear. While some studies suggest fundamentally inhibitory influence of L6CTs over first-order thalamus, potential complex, frequency-dependent effects have not been investigated in vivo. Moreover, how L6CTs affect higher-order nuclei in vivo has not been explored. This study utilizes various optogenetic manipulations of L6CTs with single-unit recordings from multiple thalamic nuclei in awake mice to address these questions. Our results illustrate similar effects of L6CTs on first- and higher-order visual thalamic nuclei, yet very different effects within-nucleus depending on how L6CTs are engaged. These findings suggest that L6CT modulation is not simply inhibitory by nature, but instead is dynamic and context-dependent.

Author contributions: M.A.K. and E.M.C. designed research; M.A.K. and A.D.F. performed research; M.A.K. analyzed data; and M.A.K. and E.M.C. wrote the paper.

Reviewers: M.E.B., University of Louisville; and S.M.S., University of Chicago.

The authors declare no competing interest.

[1]To whom correspondence may be addressed. Email: callaway@salk.edu.

This article contains supporting information online at https://www.pnas.org/lookup/suppl/doi:10.1073/pnas.2002080117/-/DCSupplemental.

First published May 27, 2020.

While we observe similar influences of L6CTs on the dLGN and pulvinar, different photostimulation conditions had strikingly different effects on thalamic firing rates, firing mode, and their balance with activity changes in the TRN. Our results thus provide evidence that L6CTs are capable of dynamically influencing activity in both their first- and higher-order thalamic targets.

Results

Sustained L6CT Photostimulation Suppresses Activity in the dLGN and Pulvinar In Vivo. Before turning to more controlled stimulation of L6CT neurons, we first tested whether previous effects observed in the dLGN of the anesthetized animal during sustained L6CT photostimulation are also observed in awake mice. Additionally, since L6CTs are hypothesized to play similar functional roles in both first- and higher-order thalamic nuclei (1), we wondered whether effects observed in the dLGN would also extend to the pulvinar. To address these questions, we injected an adeno-associated virus (AAV) encoding Cre-dependent ChR2-eYFP into V1 of Ntsr1-Cre GN220 transgenic mice (*Materials and Methods*). Consistent with prior reports of the specificity of the Ntsr1-Cre transgenic line (20, 21), expression of the ChR2-eYFP fusion protein was specific to V1 L6 (Fig. 1*B*). Corticothalamic axons expressing ChR2-eYFP were readily apparent in both the dLGN and pulvinar (Fig. 1*C* and *SI Appendix*, Fig. S1*A*), demonstrating that L6CTs labeled by the Ntsr1-Cre line project to both visual thalamic nuclei.

Single-unit activity was recorded in the visual thalamus of awake, head-fixed mice using high-density, multishank microelectrode arrays (22). Probes were coated with lipophilic dye (DiI) in order to visualize electrode tracks and determine which thalamic nucleus was sampled by each shank (Fig. 1*C*). Since the mouse pulvinar is not uniformly innervated by V1 (23–25), calretinin expression was used to distinguish between pulvinar subdivisions (*SI Appendix*, Fig. S1*A*). Only units recorded from shanks that passed through eYFP-labeled L6CT axons from V1 in the lateral, calretinin-negative zone of the pulvinar (24) were included for pulvinar analyses (e.g., second shank in Fig. 1*C*), while units recorded more medially were treated separately (e.g., first shank in Fig. 1*C* and *SI Appendix*, Fig. S1 *B–E*). While mice viewed either square-wave drifting gratings ("visual trials"; see *Materials and Methods*) or a gray screen ("blank trials"), ChR2-expressing cell bodies in V1 were stimulated with 1 s of sustained blue LED light at three different intensities ("low," "medium," and "high") (*Materials and Methods* and Fig. 1*A*). This allowed us to further probe the possibility that different degrees of L6CT stimulation might account for the variety of results previously observed with sustained light delivery (4, 5, 17, 18). We also conducted V1 recordings in a subset of AAV-injected Ntsr1-Cre mice to verify that sustained light delivery was activating L6CTs (*SI Appendix*, Fig. S2 *A–F*).

Consistent with prior reports in anesthetized mice (4, 5), L6CT photostimulation with sustained light delivery at all intensities significantly suppressed visually evoked firing rates (first example unit in Fig. 1*D*) ($n = 85$ single units from seven shanks in four animals, Fig. 1 *E–H*) in the dLGN of awake mice ($P \leq 0.003$ for visual trials with vs. without LED in all light conditions, Wilcoxon signed-rank tests). Suppression of spontaneous dLGN firing rates was also significant with high-level light stimulation (first example unit in Fig. 1 *D*, *Right*; population in *SI Appendix*, Fig. S3 *A–D*) ($P = 0.054$, 0.056, 0.008 for low, medium, and high LED vs. no LED). We also found that lateral pulvinar activity (first example unit in Fig. 1*I*) ($n = 173$ single units from 10 shanks in 6 animals, Fig. 1 *J–M*) was strongly suppressed by L6CT photostimulation during visual trials as well as blank trials (*SI Appendix*, Fig. S3 *E–G*) at all light levels ($P < 0.001$ for visual and blank trials in all LED conditions). In contrast, units recorded in the calretinin-expressing, medial area of the pulvinar that lacks direct L6CT input from V1 (24) were considerably less visually-responsive or modulated by LED stimulation (*SI Appendix*, Fig. S1). There was some heterogeneity among units in both thalamic nuclei (see second example units in Fig. 1 *D* and *I*), but especially in the dLGN where a subset of units that tended to be close to each other along the dorsal-ventral axis of the dLGN were strongly activated at higher light levels (Fig. 1*F*). While these strongly activated units in the dLGN obscure the average normalized peristimulus time histograms across units (Fig. 1 *G* and *L*), the majority of units in the dLGN (56 of 85, 65.88%) and lateral pulvinar (93 of 173, 53.76%) were significantly suppressed by L6CT photostimulation (Fig. 1 *H* and *M*). Consistent with some prior reports of firing-mode changes in first-order thalamus by sustained L6CT photostimulation (4, 12), all light intensities significantly decreased the rate of bursting in the dLGN (*SI Appendix*, Fig. S4*D*) ($P < 0.001$, $P < 0.001$, $P = 0.003$ for low, medium, and high LED vs. no LED, respectively). Bursting in the pulvinar also decreased with low-level photostimulation (*SI Appendix*, Fig. S4 *A* and *E*) ($P < 0.001$), but was unchanged with medium-level and increased with high-level photostimulation ($P = 0.911$, $P < 0.001$). Light-induced changes in activity were not observed in the dLGN or pulvinar units recorded from uninjected control animals (*SI Appendix*, Fig. S3 *H–N*), demonstrating that they were due solely to specific manipulation of L6CT activity. Thus, we demonstrate in vivo that visually evoked and spontaneous activity in the pulvinar, much like in anesthetized (4, 5) and awake dLGN (our data), is suppressed by sustained L6CT photostimulation.

L6CT Photostimulation Trains Reveal Frequency-Dependent Effects in the dLGN and Pulvinar. While our experiments with continuous light delivery for L6CT activation demonstrate L6CTs' ability to suppress their first- and higher-order thalamic targets, can they also modulate thalamic activity in other ways? Continuous light delivery is a relatively uncontrolled method for photostimulation, and our own V1 recordings demonstrate variable effects of continuous light on L6 units' activity that sometimes exceeded physiologically relevant levels (*SI Appendix*, Fig. S2 *C–F*). To overcome some of the shortcomings of continuous LED stimulation and to test for possible frequency-dependent influences that have been described in vitro (19), we used a train stimulation paradigm (Fig. 2*A*, 10-ms LED pulses at 1, 10, and 20 or 40 Hz for 1 s) to stimulate L6CT cell bodies during the same dLGN and pulvinar single-unit recording sessions from Fig. 1. We hypothesized that subsequent stimulation pulses in a 10-Hz stimulation train, and perhaps also at higher frequencies, would produce increasing spike outputs in the visual thalamus as demonstrated in the somatosensory system in vitro (19).

Indeed, in both the dLGN and pulvinar, we consistently observed facilitating spiking following subsequent pulses in a 10-Hz train (example units in Fig. 2 *B* and *C*). Whereas a single photostimulation pulse elicited at most a weak and short-lived response, this response increased dramatically with further 10-Hz stimulation pulses. The facilitation effect for each unit can be quantified by comparing the number of spikes following any pulse in the train to the number of spikes after the first pulse; thus, spike count ratios greater than 1 indicate facilitating spiking. Of the units recorded in the dLGN and pulvinar that exhibited spiking responses to individual 10-Hz light pulses (52 of 85 and 158 of 173 units considered "Hz-activated" in the dLGN and pulvinar, respectively) (*SI Appendix*, *Additional Methods*), the majority had spike count ratios (pulse 2/pulse 1) much greater than 1, and median spike count ratios were greater than 1 for all subsequent pulses (Fig. 2 *D* and *H*) ($P < 0.002$, sign test). These same signatures of facilitating spiking were absent from laminar recordings in V1 (*SI Appendix*, Fig. S2 *J* and *L*), indicating that this phenomenon is particular to L6CT (as opposed to intracortical) synapses. Notably, the example pulvinar unit in Fig. 2*C* is the same unit depicted in Fig. 1 *I*, *Upper*; while it was strongly suppressed by

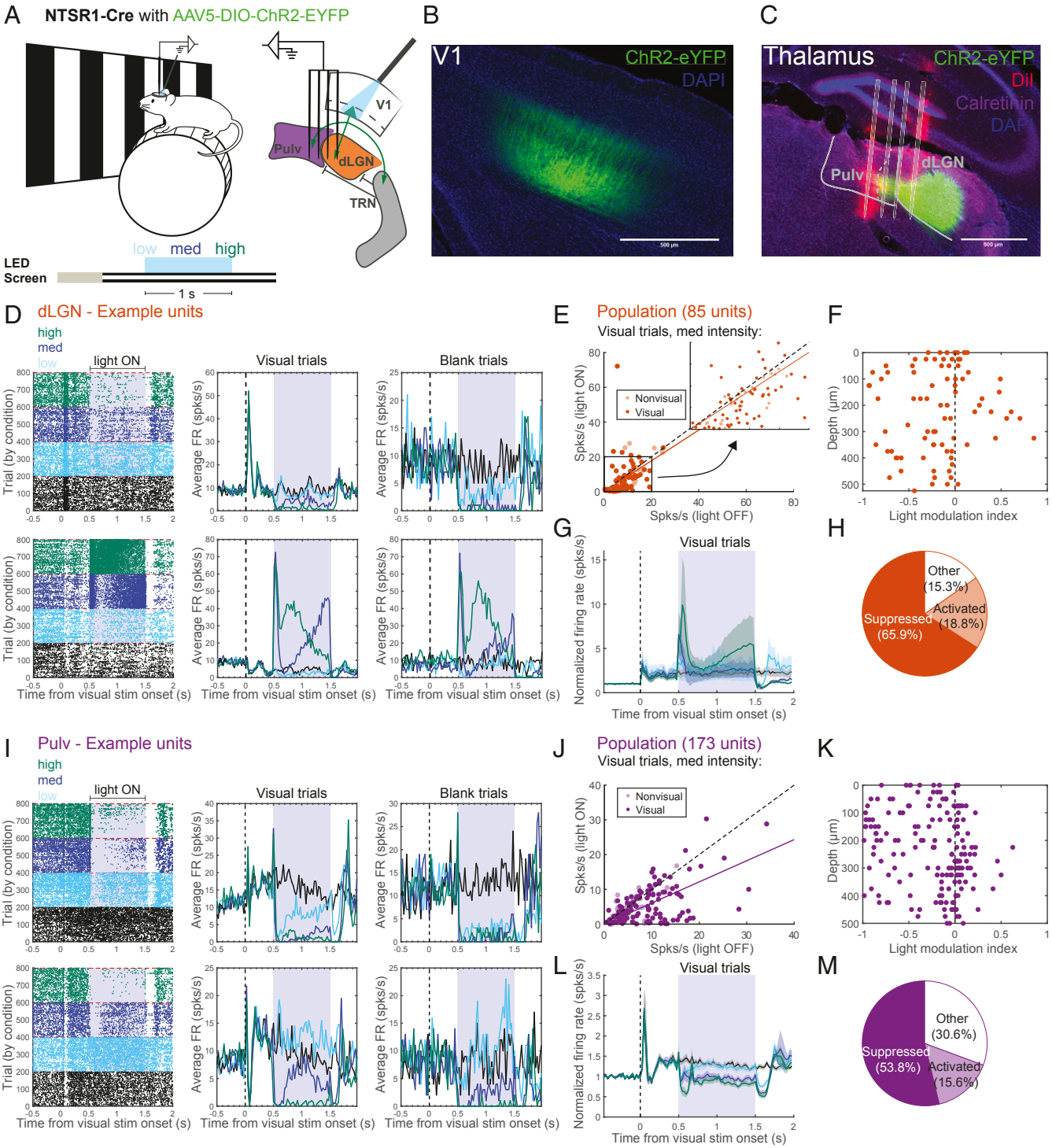

Fig. 1. L6CT photostimulation with continuous light delivery suppresses activity in the dLGN and pulvinar in vivo. (*A*) Experimental design. (*Left*) Diagram of the experimental set-up and trial structure for visual and LED stimulation. (*Right*) Schematic of the L6CT circuit, indicating recording and LED stimulation locations. (*B*) Coronal section depicting ChR2-eYFP cell body expression in V1 L6 and apical dendrites in L4 of a Ntsr1-Cre mouse injected with AAV5-DIO-ChR2-eYFP. (Scale bar, 500 μm.) (*C*) Coronal section of the visual thalamus, depicting ChR2-eYFP$^+$ axon terminals in the dLGN and pulvinar. Recording tracks from a four-shank probe are labeled with DiI (red). Immunohistochemical staining for calretinin (purple) provides borders from lateral pulvinar to dLGN and medial pulvinar. (Scale bar, 500 μm.) (*D*) Two example dLGN units. (*Left*) Raster plots with trials organized by LED condition (trials with different conditions were interspersed during the actual experiment). The shaded area indicates photostimulation period (0.5 to 1.5 s following visual stimulus onset). (*Center*) Peristimulus time histograms (PSTHs) of average firing rates during visual trials for each condition, shown over time relative to visual stimulus onset. (*Right*) PSTHs of average firing rates during blank trials (gray screen). (*E*) Average firing rates during the 1-s photostimulation period from visual trials, with versus without medium-intensity L6CT photostimulation. (*Inset*) Expanded scatter plot from area within the square (0 to 20 spikes per second). Saturated points indicate visually responsive units. (*F*) Light modulation index (<0 suppressed, >0 activated) by depth (distance from highest channel on the probe with a visually responsive unit). (*G*) Average normalized PSTH (normalized to each unit's prestimulus firing rate) across all the dLGN units. Shading indicates ±1 SEM. (*H*) Proportions of units that were significantly suppressed or activated in two or more conditions (units not passing this criteria considered "other"). (*I–M*) Same as *D–H* but for units recorded in the lateral pulvinar.

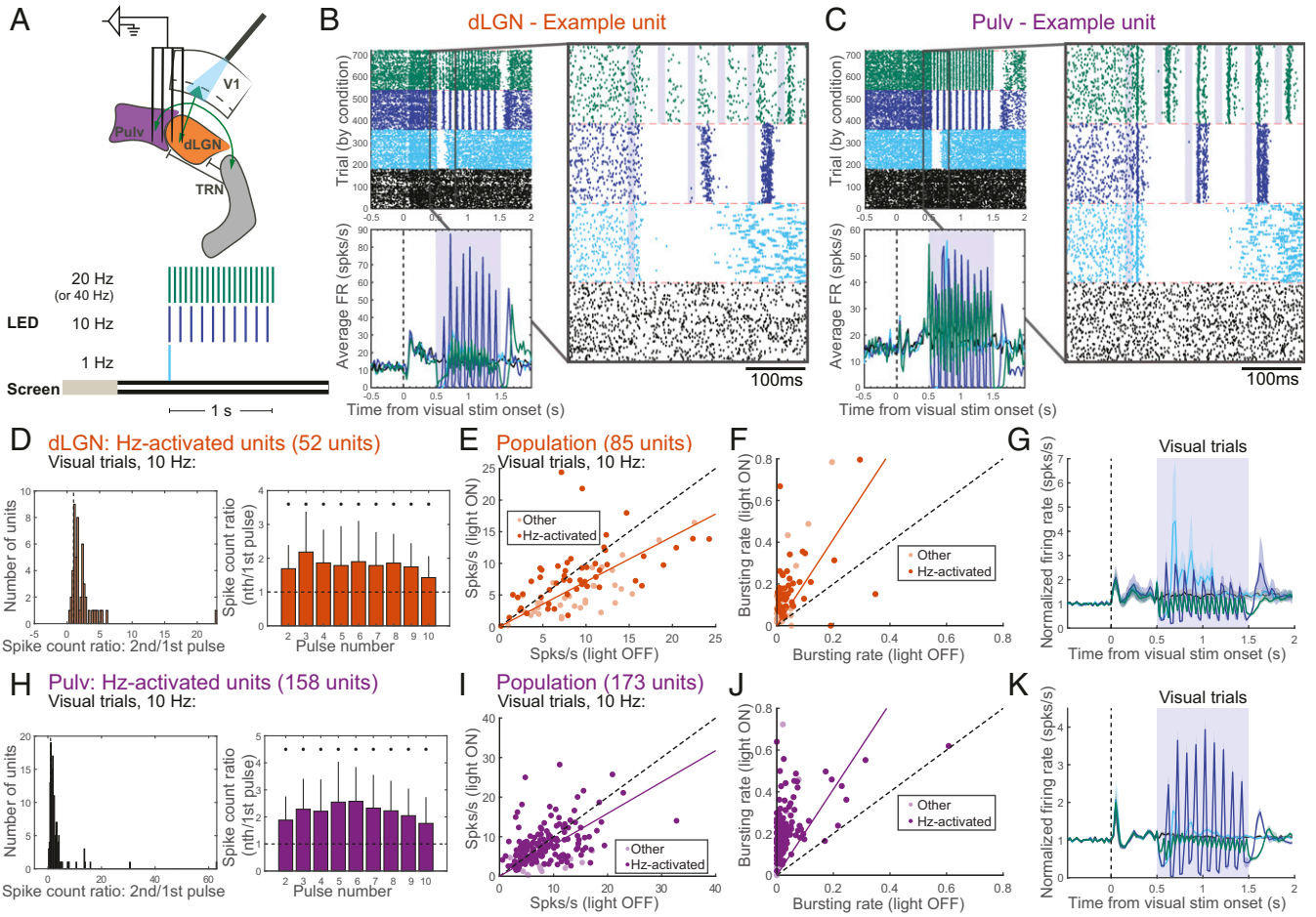

Fig. 2. Photostimulation of L6CTs at 10 Hz facilitates spiking and increases bursting in the dLGN and pulvinar. (*A*) Diagram of photostimulation and dLGN/pulvinar recording configuration and trial structure for visual and LED stimulation. (*B*) An example unit recorded in the dLGN. (*Left*) Raster plot (*Upper*) and PSTH of average firing rates across visual trials (*Lower*). (*Right*) Zoomed-in image of boxed part of raster plot (100 ms before to 300 ms after LED photostimulation onset). Shaded rectangles indicate 10-ms photostimulation pulses. (*C*) Same as *B* but for an example unit recorded in lateral pulvinar (same example unit as in Fig. 1 *I*, *Upper*). (*D*) Quantification of facilitating spiking during 10-Hz photostimulation trials across Hz-activated units in the dLGN (see *SI Appendix, Additional Methods* for "Hz-activated" unit classification). (*Left*) Histogram of spike count ratios (spike outputs following the second photostimulation pulse relative to the first in a 10-Hz train). (*Right*) Median spike count ratios across Hz-activated units, comparing spike outputs following photostimulation pulses 2 to 10 relative to the first pulse. Asterisks indicate ratios significantly different from 1 ($P < 0.002$, sign test), and error bars indicate interquartile range. (*E*) Average firing rates during the 1-s photostimulation period from visual trials, with versus without 10-Hz photostimulation. Saturated points indicate Hz-activated units included in quantification in *D*. (*F*) Average bursting rates (number of spikes that occurred during bursts/total number of spikes during 1-s photostimulation period across trials) for all units during visual trials with versus without L6CT photostimulation. (*G*) Average normalized PSTH from visual trials across all dLGN units. Shading indicates ±1 SEM. (*H–K*) Same as *D–G* but for the pulvinar.

sustained photostimulation, it exhibited facilitating spiking when driven by 10-Hz photostimulation. In fact, the majority of units in each thalamic nucleus that were significantly suppressed by sustained L6CT photostimulation demonstrated spike facilitation (spike count ratio >1) with 10-Hz photostimulation (30 of 56 and 78 of 93 in the dLGN and pulvinar, respectively). Some thalamic units (like those depicted in Fig. 2 *B* and *C*) also exhibited facilitating spiking at 20 Hz, but this was less consistent across units (*SI Appendix*, Fig. S5 *A–C*).

While facilitatory spiking was observed in both the dLGN and pulvinar directly following the photostimulation pulses, the effects of 10- to 20-Hz L6CT photostimulation on average thalamic firing rates across the full photostimulation period were, if anything, significantly suppressive in the dLGN (Fig. 2*E*) ($P = 0.07$, $P < 0.001$, $P < 0.001$ for 1 Hz, 10 Hz, and 20 to 40 Hz vs. no LED in visual trials, $P \leq 0.004$ in blank trials, Wilcoxen signed-rank tests) and approaching significance in the pulvinar (Fig. 2*I*) ($P = 0.001$, $P = 0.054$, $P < 0.001$ in visual trials, $P < 0.001$, $P = 0.068$, and $P < 0.001$ in blank trials) due to the bursting nature of their spike outputs, which closely followed the stimulation pulses. In fact, and in contrast to the effects of continuous L6CT photostimulation, the incidence of burst (as opposed to tonic) spikes increased dramatically under each train photostimulation condition in both the dLGN (Fig. 2*F* and *SI Appendix*, Fig. S4*H*) ($P < 0.001$ for 1 Hz, 10 Hz, and 20 Hz) and pulvinar (Fig. 2*J* and *SI Appendix*, Fig. S4 *B* and *I*) ($P \leq 0.001$). Therefore, moderate-frequency (10 Hz) L6CT photostimulation profoundly alters the firing mode and facilitates the spiking responses of their thalamic targets (Fig. 2 *G* and *K*), even among those which are suppressed by the same pathway under different conditions.

L6CT Axon Terminal Stimulation Does Not Suppress the dLGN and Pulvinar. To begin to explore potential circuit mechanisms underlying the context-dependent effects of L6CT photostimulation, we recorded from the dLGN and pulvinar using a two-shank "optrode" (*SI Appendix, Additional Methods* and Fig. 3 *A* and

F) that delivers blue light at the same site as the recording contacts (22). We hypothesized that by directly photostimulating ChR2-expressing L6CT axon terminals within the dLGN and pulvinar instead of their cortical cell bodies, the TRN would not be directly engaged and thus inhibition of the dLGN and pulvinar would be greatly reduced. Indeed, sustained (1 s) L6CT axon terminal stimulation elicited responses in the dLGN and pulvinar that were very different from what we previously observed with L6CT cell body stimulation (example units in Fig. 3 *B* and *G*; dLGN and pulvinar populations in Fig. 3 *E* and *J*). In experiments that included at least one shank in the dLGN ($n = 88$ single-units from five shanks in four animals), light levels had to be carefully titrated because aberrant activity was observed in the dLGN if the light intensity was too high (*SI Appendix, Additional Methods*). This likely reflects the much higher density of L6CT axon terminals in the dLGN versus pulvinar (14). Because of this, lower light levels were used in recordings that included the dLGN, and in these instances the ramp-like increase in activity in the pulvinar was largely absent (*SI Appendix*, Fig. S6 *A–D*). Under these stimulation conditions, effects of terminal stimulation on dLGN activity were variable (Fig. 3*C*) ($P = 0.316$, $P = 0.003$, and $P = 0.498$, visual trials with low, ramp to high, and high LED vs. no LED; $P = 0.002$, $P < 0.001$, $P = 0.752$, blank trials). In experiments where both recording shanks were in the pulvinar (Fig. 3*F*) ($n = 129$ single-units from six shanks in three animals), higher light levels resulted in significant enhancement of pulvinar activity (Fig. 3*H*) ($P = 0.001$ [reduced activity], visual trials with low LED vs. no LED; $P = 0.067$, $P < 0.001$ [increased activity], visual trials with med and high LED vs. no LED; $P = 0.185$, $P < 0.001$, $P < 0.001$ [increased activity], blank trials with low, medium, and high LED vs. no LED). As with the subset of facilitated units in the dLGN from cell body stimulation (Fig. 1*F*), units that were activated by L6CT axon terminal stimulation in both nuclei were also spatially clustered along the dorsal-ventral axis (Fig. 3 *D* and *I*). Similar to the effects of L6CT cell body train stimulation (Fig. 2), the rate of bursting was also significantly increased by terminal stimulation in both the dLGN and pulvinar (*SI Appendix*, Fig. S6 *E–G*) ($P < 0.001$). These changes in thalamic activity were not seen in an optrode recording from a control mouse (*SI Appendix*, Fig. S6 *H–K*), demonstrating that they were not due to the light itself or to damage from the optrode.

Overall, stimulation of L6CT terminals elicited similar changes to visually evoked and spontaneous activity in the dLGN and pulvinar (Fig. 3 *E* and *J*), and these changes were qualitatively very different from the activity changes recorded in the dLGN and pulvinar following L6CT cell body stimulation (Fig. 1). Although L6CT terminal stimulation may have antidromically activated L6CT cell bodies (26), the fact that the L6CT cell body versus terminal photostimulation evoked very different effects on recorded thalamic activity argues that antidromic activation, if present, was weak. Thus, these results demonstrate that the potent inhibitory effects observed from continuous L6CT cell body photostimulation are a consequence of the larger L6CT circuit, likely including the TRN.

Consistent with the known facilitating nature of direct L6CT-dLGN projections (15, 27), 10- to 20-Hz train stimulation of L6CT axon terminals also produced spike facilitation and increased bursting in the dLGN (*SI Appendix*, Fig. S5 *E–I*). The absence of facilitation by terminal stimulation in the lateral pulvinar (*SI Appendix*, Fig. S5 *J–N*) may be due to multiple factors relating to the lower density of terminals in the pulvinar relative to the dLGN (14). First, light levels in these experiments were optimized for the dLGN, which may have been suboptimal for pulvinar. Second, ChR2 delivered to axons has been shown to incompletely recruit axons under moderate-to-high (10 to 40 Hz) stimulation conditions, which can cause decreasing axon activation and postsynaptic responses that resemble short-term depression even at nondepressing synapses (28). Therefore, these terminal stimulation experiments further point toward both the TRN and local synaptic properties (i.e., facilitation) in mediating the frequency-dependent responses we observed with L6CT cell body stimulation.

L6CT Photostimulation Activates the Visual Sector of the TRN and Also Causes Frequency-Dependent Spike Facilitation. To more directly assess the role of the TRN in the L6CT circuit in vivo, we recorded single-unit activity in the visual sector of the TRN (visTRN) with the same L6CT cell body stimulation conditions as for the dLGN and pulvinar recordings (Fig. 4*A*). As one would expect if recordings were well-targeted to the visTRN (Fig. 4*B*), more than half (59.38%) of units were significantly visually responsive, and the majority (62.50%) exhibited fast-spiking profiles, in contrast to in the dLGN (11.76%) and pulvinar (1.73%). Since the GABAergic visTRN receives axon collaterals from L6CTs in V1 (13) and thus provides disynaptic inhibition to both the dLGN and pulvinar (29), we hypothesized that the dominant effects of sustained L6CT photostimulation on the visTRN activity would be opposite of those on the dLGN and lateral pulvinar (i.e., excitatory). Moreover, since L6CT-TRN synapses are also facilitating (27, 30), we predicted that moderate-frequency L6CT stimulation would cause similar spike facilitation in the visTRN as in the dLGN and pulvinar.

Consistent with a role for disynaptic inhibition through the visTRN in suppressing the dLGN and pulvinar during sustained L6CT cell body stimulation, many units in the visTRN were rapidly and strongly activated under these conditions (example unit in Fig. 4*C*) (population, $n = 32$ single-units from four penetrations in three animals, Fig. 4 *D–G*). At the population level, both visually evoked and spontaneous firing rates were significantly increased with L6CT photostimulation at all light levels during visual trials (Fig. 4*D*) ($P = 0.029$, $P = 0.023$, $P = 0.003$ for low, medium, and high LED vs. no LED) and approached significance in blank trials ($P = 0.014$, $P = 0.050$, $P = 0.054$). Similar to observations in the dLGN and pulvinar, the rate of bursting was also significantly reduced with low- and medium-intensity L6CT stimulation (*SI Appendix*, Fig. S4*F*) ($P = 0.045$, $P = 0.024$, $P = 0.754$ for low, medium, and high LED vs. no LED). Average visTRN population activity was increased by L6CT stimulation in a graded manner for the full duration of the photostimulation period (Fig. 4*F*), and the majority (17 of 32, 53.13%) of units were significantly activated (Fig. 4*G*). Importantly, the activation latency of the visTRN population by L6CT photostimulation (Fig. 4*F*) was the same as in the dLGN (12 ms) (Fig. 1*G*), which argues that the visTRN was engaged monosynaptically rather than indirectly by its reciprocal connections with the dLGN and pulvinar. Therefore, since the visTRN is rapidly activated during sustained L6CT photostimulation and provides GABAergic input to the dLGN and pulvinar, it will provide disynaptic inhibition to suppress the dLGN and pulvinar under these sustained stimulation conditions.

We also observed excitatory, and in fact facilitating, responses in the visTRN from 10-Hz L6CT photostimulation trains (Fig. 5 *A–C*) ($P < 0.05$). As with the dLGN and pulvinar, 20 Hz was not as effective at facilitating visTRN spiking (*SI Appendix*, Fig. S5*D*), yet all conditions (1 to 20 Hz) strongly increased the rate of bursting (Fig. 5*E* and *SI Appendix*, Fig. S4*J*) ($P < 0.001$, $P < 0.001$, and $P = 0.016$ for 1 Hz, 10 Hz, and 20 Hz, respectively). Overall, the cumulative effect of L6CT train stimulation on the visTRN (Fig. 5*F*) is virtually identical to that on the dLGN (Fig. 2*G*) and on the pulvinar (Fig. 2*K*). This similarity between the dLGN/pulvinar and visTRN responses to L6CT train stimulation, compared to their opposite responses (suppression vs. excitation) to sustained cell body stimulation (Fig. 1 vs. Fig. 4), suggests that activity in the dLGN and pulvinar more closely reflects their direct, excitatory inputs under moderate-frequency (e.g., 10 Hz) stimulation conditions, whereas the inhibitory pathway through the visTRN dominates under sustained conditions. In other words, these

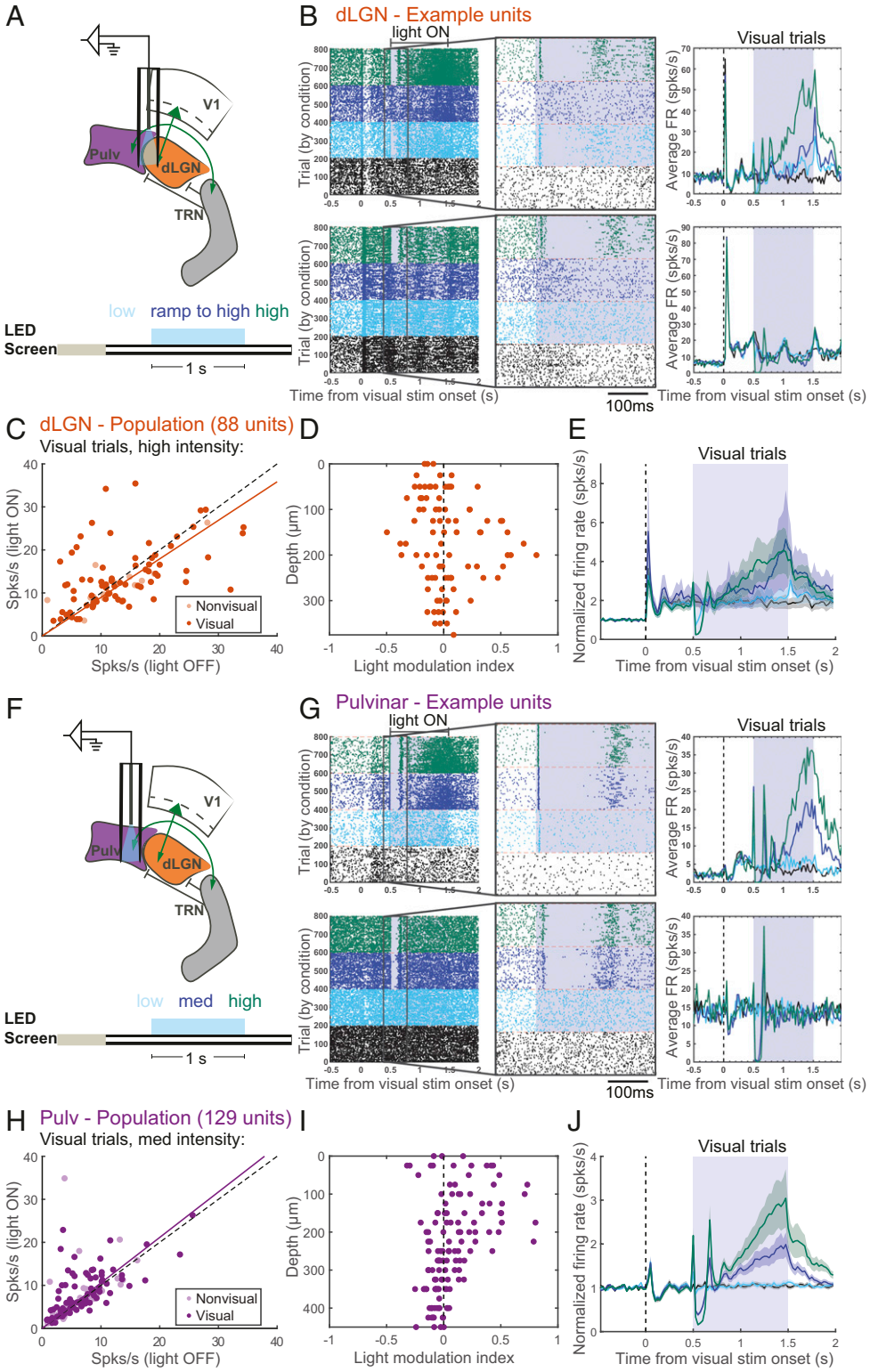

Fig. 3. Photostimulation of L6CT axon terminals in the dLGN/pulvinar does not suppress activity in visual thalamic nuclei. (*A*) Diagram of optrode configuration and trial structure for visual and LED stimulation. (*B*) Two example dLGN units. (*Left*) Raster plots. (*Center*) Zoomed-in images of boxed parts of raster plots (from 100 ms before to 300 ms after LED stimulation onset). (*Right*) PSTHs of average firing rates during visual trials. (*C*) Average firing rates during the 1-s photostimulation period from visual trials, with versus without high-intensity L6CT photostimulation. (*D*) Light modulation index by depth within the dLGN. (*E*) Average normalized PSTH from visual trials across all dLGN units. Shading indicates ±1 SEM. (*F–J*) Same as *A–E* but for units recorded in lateral pulvinar, during experiments in which the optrode was entirely in the pulvinar and higher light levels were used (*SI Appendix, Additional Methods*).

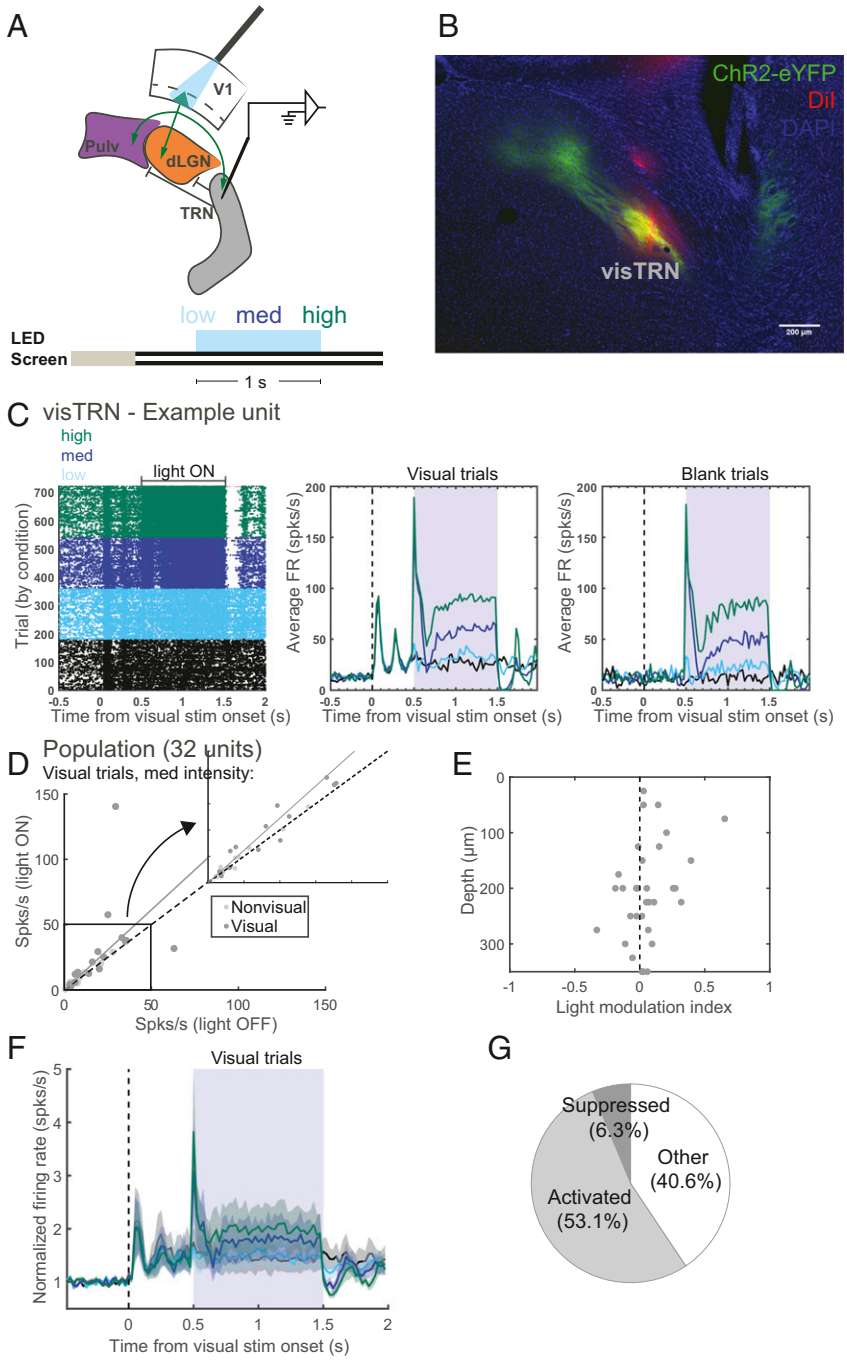

Fig. 4. L6CT cell body photostimulation with continuous light delivery activates units in the visTRN. (*A*) Diagram of photostimulation and visTRN recording locations and trial structure for visual and LED stimulation. (*B*) Coronal section depicting ChR2-eYFP$^+$ axon terminals in the visTRN from a Ntsr1-Cre mouse injected with AAV-DIO-ChR2-eYFP. The DiI track from the recording probe (red) overlaps with the L6CT axon terminal field (green). (Scale bar, 200 μm.) (*C*) Raster plot (*Left*) and PSTHs from visual trials (*Center*) and from blank trials (*Right*) for an example unit recorded in the visTRN. (*D*) Average firing rates during the 1-s photostimulation period from visual trials, with versus without medium-intensity L6CT photostimulation. (*Inset*) Expanded scatter plot from area within the square (0 to 50 spikes per second). (*E*) Light modulation index by depth within the visTRN. (*F*) Average normalized PSTH across all visTRN units. Shading indicates ±1 SEM. (*G*) Proportions of units which were significantly suppressed or activated in two or more photostimulation conditions.

parallel monosynaptic excitatory and disynaptic inhibitory pathways from L6 to first- and higher-order thalamus are dynamically opposed, which can lead to highly flexible, context-dependent effects.

Discussion

We set out to investigate how L6CTs influence first- and higher-order thalamus, using the visual system as a model. While these corticothalamic neurons are thought to serve modulatory roles in sharpening sensory responses and enhancing thalamocortical transmission in first-order thalamus (31), how they might accomplish such functions through their different excitatory and inhibitory routes to their thalamic targets is unclear. Moreover, the nature of the pathway from L6 to higher-order thalamic nuclei, like the mouse pulvinar, has not previously been explored, leaving

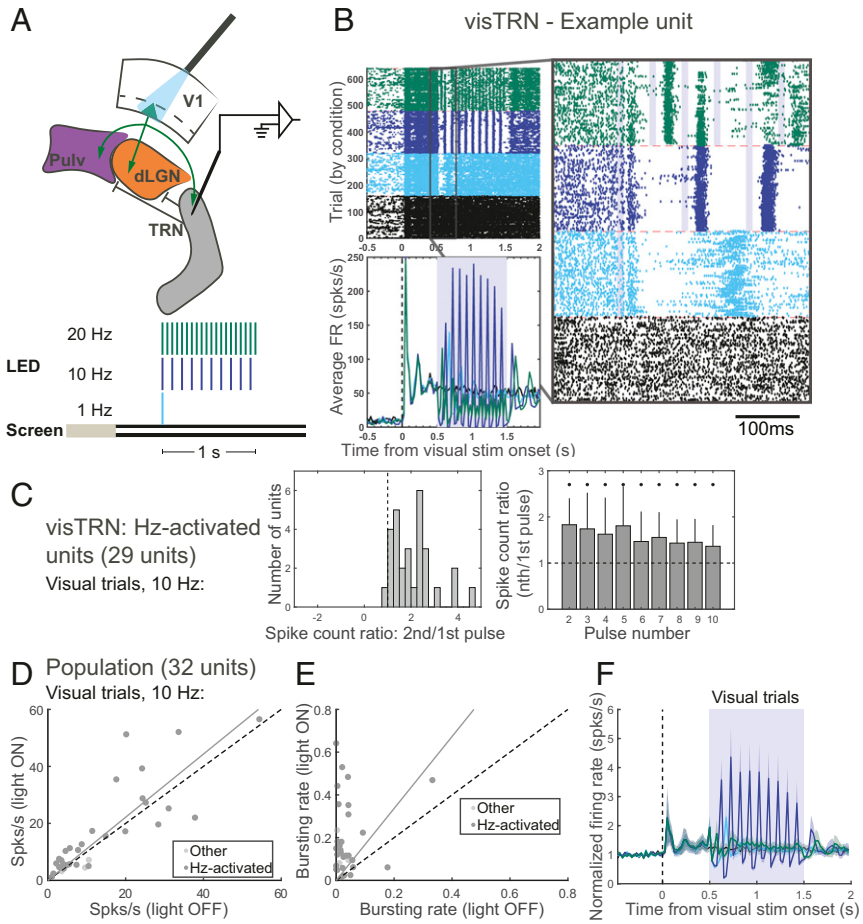

Fig. 5. Photostimulation of L6CTs at 10 Hz also facilitates spiking and increases bursting in the visTRN. (*A*) Diagram of photostimulation and visTRN recording configuration and trial structure for visual and LED stimulation. (*B*) An example unit recorded in the visTRN. (*Left*) Raster plot (*Upper*) and PSTH of average firing rates across visual trials (*Lower*). (*Right*) Zoomed-in image of boxed part of raster plot (100 ms before to 300 ms after LED photostimulation onset). Shaded rectangles indicate 10-ms photostimulation pulses. (*C*) Quantification of facilitating spiking during 10-Hz photostimulation trials across Hz-activated units in the visTRN. (*Left*) Histogram of spike count ratios (spike outputs following the second photostimulation pulse relative to the first in a 10-Hz train). (*Right*) Median spike count ratios across Hz-activated units, comparing spike outputs following photostimulation pulses 2 to 10 relative to the first pulse. Asterisks indicate ratios significantly different from 1 ($P < 0.05$, sign test), and error bars indicate interquartile range. (*D*) Average firing rates during the 1-s photostimulation period from visual trials, with versus without 10 Hz photostimulation. Saturated points indicate Hz-activated units included in quantification in *C*. (*E*) Average bursting rates for all units during visual trials with and without L6CT photostimulation. (*F*) Average normalized PSTH from visual trials across all visTRN units. Shading indicates ±1 SEM.

many unanswered questions as to how these corticothalamic neurons might exert similar or dissimilar modulatory control over different classes of thalamic nuclei.

Using high-density multielectrode recordings with optogenetics in awake, head-fixed mice, we find very similar effects on both the dLGN and pulvinar with L6CT photostimulation, but even within nuclei these effects vary greatly with the manner and degree of stimulation. Sustained optogenetic activation of L6CTs in V1 with different levels of continuous light strongly suppresses visually evoked and spontaneous activity in the dLGN and pulvinar, yet controlled 10-Hz stimulation of this same population leads to facilitating spiking in both areas. These activity changes are accompanied by changes in burst versus tonic modes of firing, which is consistent with previous reports that corticothalamic feedback can modulate thalamic firing mode (7, 8, 11, 12, 32). Remarkably, we also observed similar facilitating spiking at 10 Hz in the visTRN, yielding virtually indistinguishable effects between the visTRN and pulvinar/dLGN with L6CT train photostimulation. This stands in stark contrast to the effects on the visTRN and pulvinar/dLGN under sustained stimulation conditions, which were opposite in sign. These findings demonstrate the highly dynamic nature of these connections, whereby the relative balance between excitatory and inhibitory input to pulvinar and the dLGN and the mode of thalamic firing can shift depending on the context of corticothalamic engagement. Therefore, describing the overall effect of the L6CT pathway as simply suppressive or excitatory would fail to capture the functional nuance of this circuit.

Effects of L6CT Activation Depend on the Degree and Manner of Their Activation. Previous optogenetic experiments using Ntsr1-Cre transgenic mice under anesthesia with continuous light delivery describe a net-suppressive influence of L6CT activation on the first-order visual thalamic nucleus dLGN (4, 5). We replicate these findings in awake mice and show similar effects in the pulvinar. However, other effects of L6CT optogenetic stimulation have been reported in other species and other sensory systems; in particular, no change in dLGN firing rates in anesthetized ferret (10) and increased activity in first-order auditory and somatosensory thalamic nuclei (17, 18). While these discrepant findings could plausibly be attributed to differences between species and sensory systems, they could also be caused by methodological incongruities. Since the majority of these studies used continuous light delivery for

L6CT photostimulation, the intensity and duration of light stimulation, as well the level of viral expression, could all influence their reported observations. For example, although we found significant population-level suppression of thalamic activity with each of our chosen light intensities, there was some heterogeneity, such that some units' activity changed in opposite directions with different light intensities (e.g., *Bottom* example units in Fig. 1 *D* and *I*). Thus, in combination with our train stimulation experiments with the same population of neurons, our results can help reconcile some of these prior conflicting findings by illustrating how the complex nature of L6CT circuitry can lead to very different downstream effects under different contexts of L6CT activity. This is particularly relevant in light of the fact that L6CT neurons have very low spontaneous firing rates, are highly orientation-tuned (33), and can fire at rates around 10 Hz in vivo in response to their preferred visual stimuli (34). Brain states, such as arousal, have also been shown to increase L6CT activity (34). Therefore, our findings suggest that different degrees of L6CT engagement under normal physiological conditions and in different behavioral contexts could have significant ramifications for cortico-thalamocortical signaling.

Another important factor that may determine how L6CTs influence their thalamic targets is their topographic alignment. A limitation of ours and other rodent L6CT optogenetic studies (4, 5, 12, 17, 18) is the use of broad ChR2 expression and photoactivation of many L6CTs across retinotopic, tonotopic, or somatotopic locations. Some evidence suggests that inhibition is broader than topographically aligned excitation in cat dLGN (35) and rat VPm (36). Thus, it is entirely possible that our broad activation of L6CTs throughout V1, our use of full-field visual stimuli, and simultaneous single-unit recordings from different retinotopic locations in the thalamus may have biased us toward observing suppressive effects with sustained L6CT photostimulation in V1. Future studies, perhaps in other species (e.g., ferret, nonhuman primate) with larger cortices and finer retinotopic maps or with more sophisticated methods for targeted optogenetic stimulation, could directly test the possibility that the relative balance between monosynaptic excitatory and disynaptic inhibitory pathways in vivo also depends on the retinotopic alignment between cortical and thalamic cells.

Potential Mechanisms Underlying the Dynamic Nature of Corticothalamic Pathways. A major strength of this study is our investigation of how L6CTs impact activity in their first- and higher-order thalamic targets under a variety of different conditions in an awake animal. Our combination of recordings in the dLGN, pulvinar, and visTRN have allowed us to explore how these circuit components are recruited under various photostimulation conditions, yet we are limited by our in vivo extracellular recording methodology in capturing all possible mechanisms underlying our observed effects. For example, the patterns of activity we see are also likely to be influenced by the reciprocal excitatory/inhibitory connections between the visTRN and both the dLGN and pulvinar (37, 38). Thalamic inhibition could also come from local inhibitory interneurons which, although quite rare in the rodent thalamus and especially in the pulvinar (39), are innervated by L6CTs (27, 40). Nevertheless, the lack of pronounced suppression with axon terminal (Fig. 3) compared to cell body (Fig. 1) photostimulation suggests that thalamic interneurons are not sufficient for (but likely contribute to) the suppressive effects we observe under the latter condition.

Meanwhile, the consistency of our findings with prior in vitro work (19) allows us to speculate on likely synaptic mechanisms underlying the frequency-dependent effects we observe. First, short-term facilitation at L6CT synapses is a robust and well-described phenomenon and an important component of frequency-dependent spiking observed in the somatosensory slice preparation (19). Excitatory synaptic inputs from L6CTs to dLGN neurons have also been shown to persistently facilitate with moderate-to-high frequency (up to ∼25 Hz) electrical stimulation of the corticogeniculate pathway in vitro (41, 42) and in the anesthetized cat (43), as well as to pulvinar neurons in vitro (15). Based on our observations of spike facilitation in the visTRN with 10-Hz L6CT photostimulation, which is consistent with the known facilitating nature of these synapses (4, 19, 27, 30), one might have predicted that facilitating inhibition from the TRN would balance with facilitating excitation from L6CTs to produce consistent (rather than facilitating) spike outputs in the dLGN and pulvinar. Instead, we also observed robust spike facilitation in the dLGN and pulvinar with 10-Hz stimulation. One possible explanation is that L6CT-TRN facilitation is weaker than at L6CT-relay cell synapses (19, 27, 30), which would lead to net-facilitation of the monosynaptic excitatory pathway overall. Another potential explanation is that GABAergic synapses from the TRN to thalamic relay neurons exhibit prominent synaptic depression (19), which would allow the relative influence of disynaptic inhibition through the TRN to weaken overall with higher-frequency L6CT activity. Thus, we suspect that facilitating excitation and depressing inhibition through the TRN are both important synaptic mechanisms underlying our frequency-dependent effects.

Still other mechanisms could also be at play that are not mutually exclusive with the previously described circuit and synaptic contributions. For example, thalamic neurons' intrinsic properties, and in particular the presence of T-type calcium channels that lead to bursting when "deinactivated" at hyperpolarized membrane potentials (44, 45), may also contribute to the frequency-dependent effects we see. In fact, we observed a pronounced shift toward increased bursting during train photostimulation experiments (Figs. 2 *F* and *J* and 5*E* and *SI Appendix*, Fig. S4 *G–J*). These intrinsic properties likely account for the characteristic rebound spiking (and increased bursting) we observed in all three thalamic nuclei following ∼100 ms of silenced activity with 1-Hz photostimulation (Fig. 2 *B* and *C* and 5*B* and *SI Appendix*, Fig. S4 *G–J*), which corresponds to the approximate time for T-type calcium channels to become deinactivated by hyperpolarizing input (from the TRN, for example) and trigger a shift into burst mode (44, 45). Still, we hypothesize that these intrinsic burst properties are not sufficient on their own for the spike facilitation we observe with 10-Hz photostimulation because higher-frequency (20 Hz) photostimulation also increased bursting (*SI Appendix*, Fig. S4 *H–J*) but did not produce spike facilitation (*SI Appendix*, Fig. S5 *B–D*). Moreover, thalamic relay neurons in vitro have been shown to exhibit spike facilitation (primarily within the first few L6CT stimulation pulses, as was the case in our experiments) even when held at hyperpolarized membrane potentials to induce a sustained burst mode of firing (19). To what extent these intrinsic properties contribute to our frequency-dependent effects could be tested directly in mice with T-type calcium channels genetically deleted (46). Overall, we suggest that multiple mechanisms (intrinsic physiological, synaptic, and circuit) all contribute to the highly dynamic nature of L6CT corticothalamic pathways.

L6CT Influences on First- vs. Higher-Order Thalamus. This study offers an investigation of how L6CTs influence their higher-order thalamic targets, such as the pulvinar in the rodent visual system, in vivo. We find that, overall, L6CT photostimulation had similar effects on the lateral pulvinar as on the dLGN that were highly dynamic and frequency-dependent. These findings are consistent with hypothesized functional similarities between L6CT projections to both first- and higher-order classes of thalamic nuclei based on their similar "modulator"-like morphological and physiological characteristics (1, 2). Nevertheless, there are some differences between L6CT projections to the dLGN and pulvinar that could have led to functional disparities. For example, while many L6CTs that project to the dLGN also

project to the pulvinar (13), those that project to both classes of thalamic nuclei are only found in lower L6 (13, 47–49). The pulvinar receives additional L6 input from other visual cortical areas, and pulvinar-projecting L6CTs in these areas are found throughout L6 (47). Thus, by restricting photostimulation to V1, we are engaging a subset and perhaps even a minority of the pulvinar's L6CT inputs. Moreover, a previous study identified a small population of L6B cells that project exclusively to higher-order thalamus, but not to first-order thalamus or TRN (50); if and how this population's functional influence on pulvinar differs from that of the traditional L6CT population would be of significant interest. Yet despite these anatomical differences, we see remarkably similar effects of L6CT photostimulation in the pulvinar and dLGN that may be indicative of fundamentally similar functions for these corticothalamic pathways.

Another distinguishing feature of higher-order compared to first-order thalamic nuclei is that L6CTs are not their only source of corticothalamic input. Higher-order nuclei like the pulvinar also receive CT projections from layer 5 (L5), and these are hypothesized to act as the primary "driving" inputs in lieu of strong input from the sensory periphery (1, 2). Given the suppressive influence of L6CTs on other cortical populations within V1 (4), it is therefore possible that the inhibitory effects we see in the pulvinar with sustained L6CT photostimulation are due not only to the engagement of the visTRN as we describe, but also to indirect suppression of the L5CT "driving" inputs. While we cannot rule out this possibility, we note that L5, including lower L5 (L5B), where subcortically projecting L5 neurons in V1 are somewhat biased to reside (51), was not fully inactivated under our light stimulation conditions (*SI Appendix*, Fig. S2*D*). Moreover, the fact that we see such similar and robustly facilitating spiking with moderate-frequency L6CT photostimulation in the pulvinar as in the dLGN cannot easily be explained by a mechanism involving L5CTs. Instead, we believe our findings provide compelling in vivo evidence of functional similarity in L6CT projections to different classes of thalamic nuclei.

Summary. Our results contribute to a broader understanding of the circuit computations underlying L6CTs' functions in both first- and higher-order sensory thalamus. Observations of visual response suppression by L6CTs in the dLGN (4, 5) has led some to suppose that this is the primary mechanism by which these corticothalamic neurons wield functional influence over their thalamic targets. However, our results suggest that L6CTs take a more nuanced approach. We propose that when only weakly or transiently activated (e.g., 1-Hz condition, Fig. 2), or when the TRN is sufficiently recruited to overpower direct excitation (e.g., by sustained L6CT stimulation, Fig. 1), L6CTs exert net-inhibition over their thalamic targets (Fig. 6*A*). However, when activated within an optimal frequency range (e.g., 10 Hz, Fig. 2), L6CTs can facilitate their targets' responses to their inputs (Fig. 6*B*). That facilitating spiking was less consistent with 20-Hz L6CT stimulation (*SI Appendix*, Fig. S5 *A–D*) than with 10 Hz suggests that the relative influence of these pathways may shift again to favor disynaptic inhibition at sufficiently high frequencies (which might more closely resemble continuous LED stimulation, *SI Appendix*, Fig. S2). Furthermore, these L6CT connections can regulate not only the level but also the mode of thalamic activity, as demonstrated by our observed changes in burst versus tonic firing under different photostimulation conditions. Our data suggest that this functional flexibility is mediated by careful balancing between the parallel excitatory and inhibitory (through the TRN) routes from cortical L6 to the dorsal thalamus, altogether allowing L6CT projections to flexibly control thalamocortical input. Since we see similar L6CT effects in both first- and higher-order visual thalamus, we expect these projections to affect not only thalamocortical transmission to V1, but also cortico-thalamocortical transfer through the pulvinar to higher-order visual cortical areas. These dynamic corticothalamic pathways could afford numerous functional and computational advantages, such as for stimulus-specific amplification (31, 41) and even higher-level representations, like perceptual decision confidence in the pulvinar as demonstrated by computational modeling of these pathways (52). With an improved understanding of the highly dynamic nature of these L6CT pathways to first- and higher-order thalamus in an awake animal, future work may be able to elucidate their role in modulating sensory processing in the context of sensory-guided behaviors.

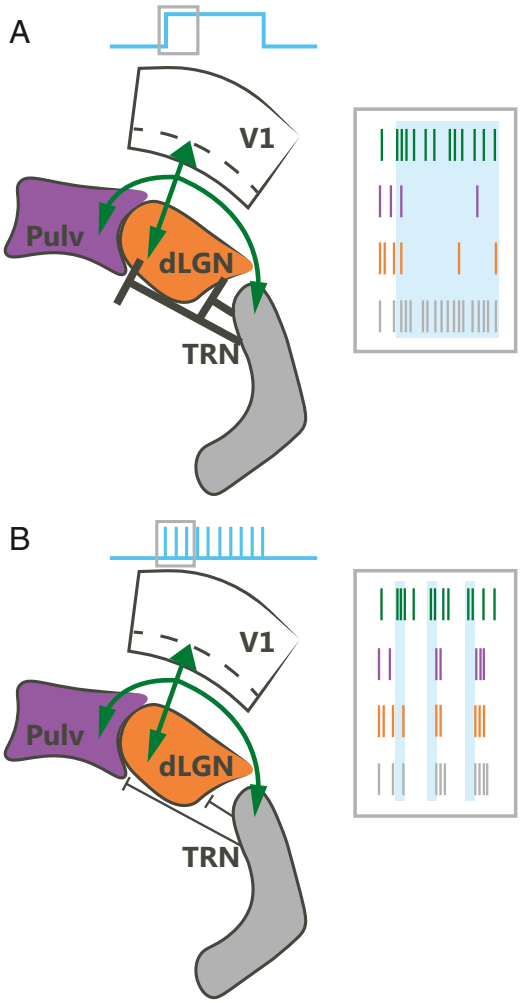

Fig. 6. Summary of how different L6CT pathways are engaged under different L6CT stimulation conditions. (*A*) With continuous light stimulation (and perhaps also with high-frequency train stimulation, e.g., ≥20 Hz) of L6CTs in V1 (green ticks), the TRN is strongly activated (gray) and thus disynaptic inhibition overpowers direct, monosynaptic excitation to result in net-suppression of the dLGN (orange) and pulvinar (purple) activity. (*B*) With moderate-frequency (e.g., 10 Hz) photostimulation of L6CTs, responses in the dLGN, pulvinar, and TRN are all similar, with facilitating and bursting spike outputs following subsequent stimulation pulses. Under these conditions, the monosynaptic excitatory pathway appears to dominate the disynaptic inhibitory pathway. Schematics of spike trains are for illustrative purposes and do not directly reflect recorded spike trains.

Materials and Methods

Animals. Male and female Ntsr1-Cre GN220 transgenic mice (GENSAT) aged 8 to 14 wk (with the exception of three mice, which were 16- to 17-wk-old) were used for experiments. Cre$^-$ animals were used for control experiments. All experimental procedures followed protocols approved by the Salk Institute Animal Care and Use Committee.

Surgeries. Mice were first anesthetized with a ketamine/xylazine mixture (100 mg/kg of ketamine and 10 mg/kg xylazine) via intraperitoneal injection and then placed in a stereotax (David Kopf Instruments Model 940 series). A small craniotomy was made over the primary visual cortex of the left hemisphere (coordinates relative to bregma: 3.20-mm posterior, 2.65-mm lateral). A total of 100 to 150 nL of AAV5-EF1a-DIO-hChR2(H134R)-eYFP was pressure-injected via Picospritzer (General Valve Corp.) or syringe through a 25- to 30-μm pipette at 1 to 2 depths, 0.3 to 0.6 mm from pial surface. AAVs were injected at an approximate rate of 20 nL/min, and the pipette was left in place for at least 5 min following injection prior to removal. Mice were returned to their cages and given 2.5 to 3 wk before experimentation. Four to 7 d before experimentation, mice underwent an acute surgery for headframe implantation. Skin was cleared away so that a circular headframe (7-mm inner diameter) could be attached with dental cement (C&B-Metabond, Parkell). A dull pipette attached to a micromanipulator (MP-285, Sutter Instrument) was used to relocate bregma and mark positions with a waterproof pen for targeting thalamus recordings (coordinates relative to bregma: 1.25- to 2.75-mm lateral, 1.8- to 1.9-mm posterior). The skull was covered with a silicone elastomer (Kwik-Cast, World Precision Instruments) and mice were given a carpofen subcutaneous injection (5 mg/kg), Ibuprofen in their water bottles, and at least 24 h undisturbed in their cages.

In Vivo Electrophysiology and Optogenetics. Prior to recordings, mice were given two to four training sessions to habituate to the running wheel. One day prior and on the day of recordings, mice were given a dilution of dexmethasone (15 mg/kg) to alleviate brain swelling. On the day of recording, mice were anesthetized with isoflurane, and a craniotomy was made over the thalamus of the left hemisphere. For cell body stimulation experiments, an additional craniotomy was made over the injection site in V1 (in two animals the cortex was heavily thinned). Mice were then head-fixed on a wheel, where they were free to run at their will and movement was tracked with a rotary encoder. Silicon microprobes (22) were coated with a 2.5 to 5% solution of DiI (D282, ThermoFisher) in distilled water or ethanol and lowered into the thalamus with a micromanipulator (MP-285, Sutter Instrument). Probe configurations used for dLGN/pulvinar recordings were 128DN and 128D (128 channels across four shanks, 775-μm vertical extent of electrodes, 150- or 330-μm separation between shanks, respectively). A custom optrode (64G configuration, 64 channels across two shanks, 300-μm separation between shanks, 525-μm vertical extent of electrodes) was used for axon terminal stimulation experiments (see *SI Appendix* for additional methods). A 64D probe (64 channels on one shank, 1.05-mm vertical extent of electrodes) was used for the visTRN recordings. For cell body stimulation experiments, a 1-mm-diameter optical fiber (0.39 NA, ThorLabs) was positioned at approximately a 50 to 60° angle from and 0.5- to 1-mm above the surface of the V1 craniotomy. The optical fiber patch cord was connected to a blue-wavelength LED driver (PlexBright LED 465 nm, Plexon), and light power was measured at the fiber tip as 0.7 to 1 mW (low), 3.5 to 4.5 mW (medium), and 6.5 to 8.5 mW (high). Multishank probes for thalamic recordings were oriented horizontally (medial-lateral). After the probe penetrated the cortical surface, agarose (2.5 to 3.5%; A9793, Sigma-Aldrich) was poured over to fill the well of the headframe holder, thus covering the probe shanks and the tip of the optical fiber. The probe was continuously lowered slowly down to ∼2.4- to 2.6-mm beneath the cortical surface over the course of ∼20 min. Once the probe was in its final position, it was allowed to sit and settle for 30 min before any data acquisition commenced. Data from all but two animals were acquired at 20 kHz with an OpenEphys acquisition system (53), connected to an Intan RHD2000 128-channel amplifier board. Data from the remaining two animals were acquired at 20 kHz with an Intan RHD2000 USB interface board.

Visual Stimulation. Visual stimuli was generated through custom MATLAB code using Psychtoolbox, as described previously (54), and presented on a 24″ LED monitor (GL2450-B, BenQ). The monitor screen was positioned 12 cm from the mouse's right eye. Visual stimuli consisted of square-wave drifting gratings at four orientations in eight directions, 0.04 cycles per degree spatial frequency, and 2-Hz temporal frequency (one experiment in one mouse at 1 Hz). A full "trial" consisted of a 0.5-s prestimulus period (gray screen), 2 s of visual stimulus presentation, and 1.5- to 2-s poststimulus period (gray screen). Twenty percent of trials were "blank" trials, in which the screen remained gray for the full trial duration.

Quantification and Statistical Analysis. Briefly, spike-sorting on extracellularly recorded data were performed semiautomatically using Kilosort (55) and manually curated with Phy (56). Only good single units (see *SI Appendix* for criteria) were used for subsequent analyses. Average firing rates were calculated from the 1-s period of photostimulation (0.5 to 1.5 s from visual stimulus onset) separately for visual and blank trials (stationary trials only) and for each light condition (no light, low, medium, high). Statistical significance of each unit's response to L6CT photostimulation was assessed using a Wilcoxen rank-sum test comparing spiking responses during the 1-s photostimulation period on all trials with and without photostimulation (separately for each photostimulation condition). Units were considered "suppressed" if their activity was significantly suppressed ($P < 0.05$ and light modulation index <0) in at least two of three conditions, or "activated" if their activity was significantly increased ($P < 0.05$ and light modulation index >0) in at least two of three conditions. Population-level statistics were performed with the Wilcoxen signed-rank test.

Additional detailed methods can be found in *SI Appendix*.

Data Availability. All relevant data and code will be made available by the authors upon reasonable request.

ACKNOWLEDGMENTS. We thank Drs. Ashley Juavinett and Pamela Reinagel for comments on the manuscript; Drs. Sotiris Masmanidis and Kwang Lee for help with optrode assembly; and other members of the E.M.C. laboratory for helpful discussions. This work was supported by NIH Grants F31 EY028853 (to M.A.K.), and R01 MH063912 and R01 EY022577 (to E.M.C.).

1. S. M. Sherman, R. W. Guillery, On the actions that one nerve cell can have on another: Distinguishing "drivers" from "modulators". *Proc. Natl. Acad. Sci. U.S.A.* **95**, 7121–7126 (1998).
2. S. M. Sherman, Thalamus plays a central role in ongoing cortical functioning. *Nat. Neurosci.* **19**, 533–541 (2016).
3. A. W. Przybyszewski, J. P. Gaska, W. Foote, D. A. Pollen, Striate cortex increases contrast gain of macaque LGN neurons. *Vis. Neurosci.* **17**, 485–494 (2000).
4. S. R. Olsen, D. S. Bortone, H. Adesnik, M. Scanziani, Gain control by layer six in cortical circuits of vision. *Nature* **483**, 47–52 (2012).
5. D. J. Denman, D. Contreras, Complex effects on in vivo visual responses by specific projections from mouse cortical layer 6 to dorsal lateral geniculate nucleus. *J. Neurosci.* **35**, 9265–9280 (2015).
6. W. Wang, I. M. Andolina, Y. Lu, H. E. Jones, A. M. Sillito, Focal gain control of thalamic visual receptive fields by layer 6 corticothalamic feedback. *Cereb. Cortex* **28**, 267–280 (2018).
7. W. Wang, H. E. Jones, I. M. Andolina, T. E. Salt, A. M. Sillito, Functional alignment of feedback effects from visual cortex to thalamus. *Nat. Neurosci.* **9**, 1330–1336 (2006).
8. M. A. Spacek, G. Born, D. Crombie, S. A. Katzner, L. Busse, Robust effects of cortical feedback on thalamic firing mode during naturalistic stimulation. bioRxiv:10.1101/776237 (20 September 2019).
9. I. M. Andolina, H. E. Jones, W. Wang, A. M. Sillito, Corticothalamic feedback enhances stimulus response precision in the visual system. *Proc. Natl. Acad. Sci. U.S.A.* **104**, 1685–1690 (2007).
10. J. M. Hasse, F. Briggs, Corticogeniculate feedback sharpens the temporal precision and spatial resolution of visual signals in the ferret. *Proc. Natl. Acad. Sci. U.S.A.* **114**, E6222–E6230 (2017).
11. I. M. Andolina, H. E. Jones, A. M. Sillito, Effects of cortical feedback on the spatial properties of relay cells in the lateral geniculate nucleus. *J. Neurophysiol.* **109**, 889–899 (2013).
12. R. A. Mease, P. Krieger, A. Groh, Cortical control of adaptation and sensory relay mode in the thalamus. *Proc. Natl. Acad. Sci. U.S.A.* **111**, 6798–6803 (2014).
13. J. Bourassa, M. Deschênes, Corticothalamic projections from the primary visual cortex in rats: A single fiber study using biocytin as an anterograde tracer. *Neuroscience* **66**, 253–263 (1995).
14. J. Li, S. Wang, M. E. Bickford, Comparison of the ultrastructure of cortical and retinal terminals in the rat dorsal lateral geniculate and lateral posterior nuclei. *J. Comp. Neurol.* **460**, 394–409 (2003).
15. J. Li, W. Guido, M. E. Bickford, Two distinct types of corticothalamic EPSPs and their contribution to short-term synaptic plasticity. *J. Neurophysiol.* **90**, 3429–3440 (2003).
16. I. Reichova, S. M. Sherman, Somatosensory corticothalamic projections: Distinguishing drivers from modulators. *J. Neurophysiol.* **92**, 2185–2197 (2004).
17. W. Guo, A. R. Clause, A. Barth-Maron, D. B. Polley, A corticothalamic circuit for dynamic switching between feature detection and discrimination. *Neuron* **95**, 180–194.e5 (2017).
18. F. P. Pauzin, P. Krieger, A corticothalamic circuit for refining tactile encoding. *Cell Rep.* **23**, 1314–1325 (2018).
19. S. R. Crandall, S. J. Cruikshank, B. W. Connors, A corticothalamic switch: Controlling the thalamus with dynamic synapses. *Neuron* **86**, 768–782 (2015).
20. S. Gong *et al.*, Targeting Cre recombinase to specific neuron populations with bacterial artificial chromosome constructs. *J. Neurosci.* **27**, 9817–9823 (2007).
21. D. S. Bortone, S. R. Olsen, M. Scanziani, Translaminar inhibitory cells recruited by layer 6 corticothalamic neurons suppress visual cortex. *Neuron* **82**, 474–485 (2014).

22. L. Yang, K. Lee, J. Villagracia, S. C. Masmanidis, Open source silicon microprobes for high throughput neural recording. *J. Neural Eng.* **17**, 16036 (2020).
23. R. Beltramo, M. Scanziani, A collicular visual cortex: Neocortical space for an ancient midbrain visual structure. *Science* **363**, 64–69 (2019).
24. N. A. Zhou, P. S. Maire, S. P. Masterson, M. E. Bickford, The mouse pulvinar nucleus: Organization of the tectorecipient zones. *Vis. Neurosci.* **34**, E011 (2017).
25. C. Bennett *et al.*, Higher-order thalamic circuits channel parallel streams of visual information in mice. *Neuron* **102**, 477–492.e5 (2019).
26. R. S. Williamson, D. B. Polley, Parallel pathways for sound processing and functional connectivity among layer 5 and 6 auditory corticofugal neurons. *eLife* **8**, e42974 (2019).
27. C. W. D. Jurgens, K. A. Bell, A. R. McQuiston, W. Guido, Optogenetic stimulation of the corticothalamic pathway affects relay cells and GABAergic neurons differently in the mouse visual thalamus. *PLoS One* **7**, e45717 (2012).
28. C. A. Hass, L. L. Glickfeld, High-fidelity optical excitation of cortico-cortical projections at physiological frequencies. *J. Neurophysiol.* **116**, 2056–2066 (2016).
29. D. Pinault, M. Deschênes, Projection and innervation patterns of individual thalamic reticular axons in the thalamus of the adult rat: A three-dimensional, graphic, and morphometric analysis. *J. Comp. Neurol.* **391**, 180–203 (1998).
30. S. J. Cruikshank, H. Urabe, A. V. Nurmikko, B. W. Connors, Pathway-specific feedforward circuits between thalamus and neocortex revealed by selective optical stimulation of axons. *Neuron* **65**, 230–245 (2010).
31. F. Briggs, W. M. Usrey, Emerging views of corticothalamic function. *Curr. Opin. Neurobiol.* **18**, 403–407 (2008).
32. D. A. McCormick, M. von Krosigk, Corticothalamic activation modulates thalamic firing through glutamate "metabotropic" receptors. *Proc. Natl. Acad. Sci. U.S.A.* **89**, 2774–2778 (1992).
33. M. Vélez-Fort *et al.*, The stimulus selectivity and connectivity of layer six principal cells reveals cortical microcircuits underlying visual processing. *Neuron* **83**, 1431–1443 (2014).
34. C. R. Stoelzel, Y. Bereshpolova, J.-M. Alonso, H. A. Swadlow, Axonal conduction delays, brain state, and corticogeniculate communication. *J. Neurosci.* **37**, 6342–6358 (2017).
35. T. Tsumoto, O. D. Creutzfeldt, C. R. Legéndy, Functional organization of the corticofugal system from visual cortex to lateral geniculate nucleus in the cat (with an appendix on geniculo-cortical mono-synaptic connections). *Exp. Brain Res.* **32**, 345–364 (1978).
36. L. Li, F. F. Ebner, Cortical modulation of spatial and angular tuning maps in the rat thalamus. *J. Neurosci.* **27**, 167–179 (2007).
37. M. Conley, I. T. Diamond, Organization of the visual sector of the thalamic reticular nucleus in galago. *Eur. J. Neurosci.* **2**, 211–226 (1990).
38. E. G. Jones, Ed., *The Thalamus*, (Plenum Press, New York, 1985).
39. M. Evangelio, M. García-Amado, F. Clascá, Thalamocortical projection neuron and interneuron numbers in the visual thalamic nuclei of the adult C57BL/6 mouse. *Front. Neuroanat.* **12**, 27 (2018).
40. S. Augustinaite, Y. Yanagawa, P. Heggelund, Cortical feedback regulation of input to visual cortex: Role of intrageniculate interneurons. *J. Physiol.* **589**, 2963–2977 (2011).
41. B. Granseth, Dynamic properties of corticogeniculate excitatory transmission in the rat dorsal lateral geniculate nucleus in vitro. *J. Physiol.* **556**, 135–146 (2004).
42. M. von Krosigk, J. E. Monckton, P. B. Reiner, D. A. McCormick, Dynamic properties of corticothalamic excitatory postsynaptic potentials and thalamic reticular inhibitory postsynaptic potentials in thalamocortical neurons of the guinea-pig dorsal lateral geniculate nucleus. *Neuroscience* **91**, 7–20 (1999).
43. S. Lindström, A. Wróbel, Frequency dependent corticofugal excitation of principal cells in the cat's dorsal lateral geniculate nucleus. *Exp. Brain Res.* **79**, 313–318 (1990).
44. H. Jahnsen, R. Llinás, Electrophysiological properties of guinea-pig thalamic neurones: An in vitro study. *J. Physiol.* **349**, 205–226 (1984).
45. H. Jahnsen, R. Llinás, Ionic basis for the electro-responsiveness and oscillatory properties of guinea-pig thalamic neurones in vitro. *J. Physiol.* **349**, 227–247 (1984).
46. M. P. Anderson *et al.*, Thalamic Cav3.1 T-type Ca2+ channel plays a crucial role in stabilizing sleep. *Proc. Natl. Acad. Sci. U.S.A.* **102**, 1743–1748 (2005).
47. M. M. Roth *et al.*, Thalamic nuclei convey diverse contextual information to layer 1 of visual cortex. *Nat. Neurosci.* **19**, 299–307 (2016).
48. M. Chevée, J. J. Robertson, G. H. Cannon, S. P. Brown, L. A. Goff, Variation in activity state, axonal projection, and position define the transcriptional identity of individual neocortical projection neurons. *Cell Rep.* **22**, 441–455 (2018).
49. J. Bourassa, D. Pinault, M. Deschênes, Corticothalamic projections from the cortical barrel field to the somatosensory thalamus in rats: A single-fibre study using biocytin as an anterograde tracer. *Eur. J. Neurosci.* **7**, 19–30 (1995).
50. A. Hoerder-Suabedissen *et al.*, Subset of cortical layer 6b neurons selectively innervates higher order thalamic nuclei in mice. *Cereb. Cortex* **28**, 1882–1897 (2018).
51. A. Groh *et al.*, Cell-type specific properties of pyramidal neurons in neocortex underlying a layout that is modifiable depending on the cortical area. *Cereb. Cortex* **20**, 826–836 (2010).
52. J. Jaramillo, J. F. Mejias, X.-J. Wang, Engagement of pulvino-cortical feedforward and feedback pathways in cognitive computations. *Neuron* **101**, 321–336.e9 (2019).
53. J. H. Siegle *et al.*, Open Ephys: An open-source, plugin-based platform for multichannel electrophysiology. *J. Neural Eng.* **14**, 45003 (2017).
54. J. H. Marshel, M. E. Garrett, I. Nauhaus, E. M. Callaway, Functional specialization of seven mouse visual cortical areas. *Neuron* **72**, 1040–1054 (2011).
55. M. Pachitariu, N. Steinmetz, S. Kadir, M. Carandini, K. D. Harris, Kilosort: Realtime spike-sorting for extracellular electrophysiology with hundreds of channels. bioRxiv: 10.1101/061481 (30 June 2016).
56. C. Rossant *et al.*, Spike sorting for large, dense electrode arrays. *Nat. Neurosci.* **19**, 634–641 (2016).